Journal of Power Sources 197 (2012) 57–64

Contents lists available at SciVerse ScienceDirect

Journal of Power Sources

journal homepage: www.elsevier.com/locate/jpowsour

A new symmetric solid oxide fuel cell with a samaria-doped ceria framework and a silver-infiltrated electrocatalyst

Ye Lin[a], Chao Su[a], Cheng Huang[a], Ju Sik Kim[b], Chan Kwak[b], Zongping Shao[a,*]

[a] State Key Laboratory of Materials-Oriented Chemical Engineering, College of Chemistry & Chemical Engineering, Nanjing University of Technology, No. 5 Xin Mofan Road, Nanjing 210009, PR China
[b] R&D Center, Samsung Advanced Institute of Technology, Samsung Electronics Co., Ltd., 416 Maetan-Dong, Yeongtong-Gu, Suwon, Gyeonggi-Do 443-742, Republic of Korea

ARTICLE INFO

Article history:
Received 26 July 2011
Received in revised form
14 September 2011
Accepted 15 September 2011
Available online 21 September 2011

Keywords:
Symmetric solid oxide fuel cell
Infiltration
Silver
Samaria-doped ceria

ABSTRACT

A new symmetric SOFC with an SDC framework and a silver-infiltrated electrocatalyst is presented for the first time in this paper. A three-electrode polarization test shows that the Ag–SDC has a low area specific resistance of 1.07 Ω cm^2 at 600 °C, a low activation energy of 85 kJ mol^{-1} and high exchange current densities of 428.2 and 129.0 mA cm^{-2} at 750 and 650 °C, respectively, when it is used as an oxygen reduction electrode. It also exhibits low polarization resistance in a humidified hydrogen atmosphere. A symmetric single cell is used in real fuel cell conditions to deliver peak power densities of 200 and 84 mW cm^{-2} at 750 and 650 °C, respectively, when humidified hydrogen is used as a fuel and ambient air is used as the cathode atmosphere. The cell still reaches a peak power density of 81 mW cm^{-2} at 750 °C when operating on CO. O_2-TPO analysis demonstrates that the Ag–SDC electrode has even better coking resistance than the pure SDC scaffold. The results indicate that Ag–SDC|SDC|Ag–SDC symmetric cells with an infiltrated silver electrocatalyst are a promising new type of fuel cell for use with both hydrogen fuel and carbon-containing fuels.

1. Introduction

The expanding demand for energy and the increasing environmental pollution resulting from the inefficient burning of fossil fuels is making it necessary to use alternative clean fuels and develop more efficient, green and sustainable ways of utilizing available energy resources. Fuel cells directly convert chemical energy stored in fuel to electric power, working much more efficiently than well established fossil fuel combustion technologies and producing lower emissions. Thus, they have attracted substantial attention recently [1–5].

Solid oxide fuel cells (SOFCs) are high-temperature devices that have ceramic electrolytes and all solid components. They have good modality and accept a wide range of fuels, including hydrogen and other, more accessible chemicals like methane, gasoline and coal [6–14]. It is believed that SOFCs are ideal for future clean power generation. Conventional SOFCs are composed of yttria-stabilized zirconia (YSZ) electrolytes, Ni–YSZ cermet anodes and $La_{0.8}Sr_{0.2}MnO_3$ (LSM) cathodes [15]. They can deliver promising power output at approximately 1000 °C using hydrogen fuel. Reducing the operating temperature to the intermediate range (i.e., 600–850 °C) is believed to be key to facilitating the widespread use of SOFC technology in our daily lives [16–19]. However, at intermediate temperatures, the state-of-the-art LSM cathodes and YSZ electrolytes exhibit insufficient electrocatalytic activity for oxygen reduction and poor ionic conductivity. Although Ni + YSZ cermet anodes exhibit excellent catalytic activity for fuel reformation, good activity for fuel electro-catalytic oxidation and good current collecting properties, they also exhibit a low tolerance for carbon deposition and poor redox stability [20–22]. These results suggest the urgent need to develop alternative cell materials and improve the cell configuration used.

Recently, Irvine et al. and Nunez et al. developed a new SOFC configuration named symmetric SOFC in which the redox stable perovskite oxide $La_{0.75}Sr_{0.25}Cr_{0.5}Mn_{0.5}O_3$ (LSCM) was used for both electrodes for a cell with a YSZ electrolyte [23,24]. The authors suggest that this new technique has several important advantages. Coke formation over the anode and sulfur poisoning when sulfur-containing hydrocarbon fuels are used can be easily eliminated or lessened by simply changing the gas flow. In addition, the identical composition of the anodes and cathodes allows them to be fired in a single step, thereby reducing fabrication costs. Later, several researchers also reported the attractive cell performance of certain symmetric SOFCs at high temperatures when composite oxides such as LSCM, $La_{0.8}Sr_{0.2}Sc_{0.3}Mn_{0.7}O_3$ and LSCM–YSZ + CeO_2 were used as the electrodes [25–31]. However, at intermediate temperatures, those oxide electrodes exhibit low electrical conductivity under a reducing atmosphere. For

* Corresponding author. Tel.: +86 25 83172256; fax: +86 25 83172242.
E-mail address: shaozp@njut.edu.cn (Z. Shao).

0378-7753/$ – see front matter © 2011 Elsevier B.V. All rights reserved.
doi:10.1016/j.jpowsour.2011.09.040

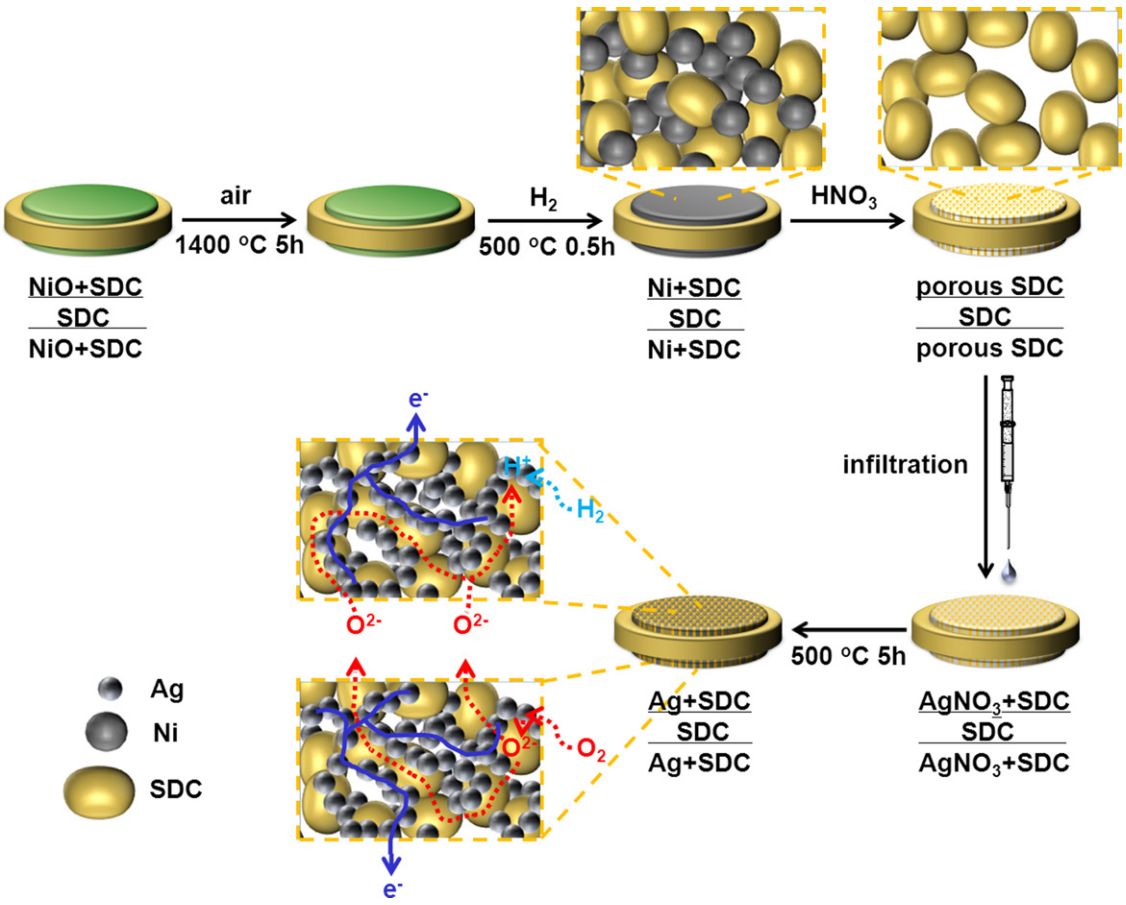

Fig. 1. A schematic used in the fabrication of silver-infiltrated symmetric SOFC with an SDC framework.

example, dense LSCM pellets have very low electrical conductivity in a hydrogen atmosphere [31], and the conductivity of porous LSCM electrodes may be as much as ten times lower. These low performance levels constitute a significant impediment to current collection. Recently, Ruiz-Morales et al. reported that a symmetric cell with the configuration of Pt|YSZ–CeO_2|YSZ|YSZ–CeO_2|Pt delivered a peak power density of 140 mW cm^{-2} at 950 °C using hydrogen as the fuel and thick YSZ as the electrolyte [32]. Although the use of Pt may solve the problem of low electrical conductivity of YSZ–CeO_2 oxide electrodes, it substantially increases the material costs. In addition, the use of YSZ as an electrolyte also limits the operation of the cell to high temperatures. The active zone of the electrode is believed to be approximately 10–20 μm from the electrolyte interface [33,34], which suggests that the precious Pt in the electrode layers may perform mainly as a current collector.

In the current study, we present a new highly coke-resistant symmetric intermediate-temperature (IT) SOFC whose entire cell is built from samaria-doped ceria (SDC). We created the cell from a dense, thick SDC electrolyte and two symmetric porous SDC layers, which we used as the backbone for the electrodes. Silver was added to the two porous SDC scaffolds using solution infiltration, with the Ag–SDC composites used separately as the anode and the cathode. The Ag–SDC electrodes show both high electrical conductivity and high oxygen reduction and hydrogen electro-oxidation. The SDC framework for the whole cell eliminates thermal mismatch and also eliminates the possibility of interfacial phase reactions between the electrolyte and the electrodes. The cell exhibited attractive performance when operated on hydrogen and carbon monoxide at intermediate temperatures.

2. Experimental

2.1. Cell fabrication

The materials used in this study for cell fabrication include $Sm_{0.2}Ce_{0.8}O_{1.9}$ (SDC), NiO and $AgNO_3$. The SDC was synthesized using an EDTA–citrate complexing sol–gel process, whereas the NiO and $AgNO_3$ were commercial products. To synthesize the SDC, $Sm(NO_3)_3{\cdot}6H_2O$ (A.R., Aladdin Reagent Co., Ltd., Shanghai, China) and $Ce(NO_3)_3{\cdot}6H_2O$ (A.R., Sinopharm Chemical Reagent Co., Ltd., Shanghai, China) were first prepared in separate aqueous solutions whose precise concentration was determined using a standard EDTA titration method. They were then mixed at the required amounts. During stirring and heating, EDTA and citric acid were added to the solution, used as successive complexing agents at a molar ratio of 1:1:2 for total metal ions:EDTA:citric acid. To avoid precipitation, the pH value of the solution was controlled at ~6 during the solution process with NH_4OH. A gel was obtained by vaporizing water from the solution at 90 °C. It was pre-fired at 250 °C and then calcined at 1000 °C for 5 h in an air atmosphere to obtain a product with the desired composition.

The procedure used for cell fabrication is schematically shown in Fig. 1. Dense SDC electrolytes were prepared via dry pressing using a stainless steel die under hydraulic pressure of 200 MPa and followed by high-temperature sintering at 1450 °C for 5 h in air. The sintered SDC pellets were then polished on both sides using attrition paper until they reached a thickness of approximately 0.4 mm. The NiO and SDC were thoroughly mixed at a weight ratio of 60 to 40 and dispersed in a mixed solution of ethylene glycol, ethanol and isopropyl alcohol via high-energy ball milling (Fritsch,

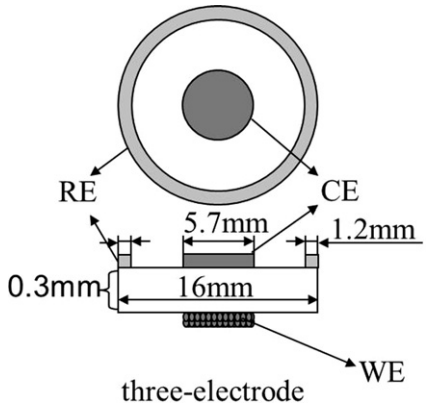

Fig. 2. A diagram of the three-electrode structure for impedance and overpotential measurements.

Pulverisette 6) at a rotational speed of 400 rpm for 0.5 h. The NiO and SDC were then deposited onto the central surface of the electrolyte in a circular pattern by the air-driven spray. The geometric surface area was 0.26 and 1.13 cm^2 for three-electrode cells and symmetric cells, respectively. The next step was to fire the cells at 1400 °C in air for 5 h. The fabricated cells were reduced in hydrogen at 500 °C for 30 min and then dropped into a diluted aqueous nitric acid solution at room temperature to extract the nickel from the electrodes and create highly porous SDC scaffolds with porosity exceeding 70 vol.%. The silver was added to the scaffolds via repeated $AgNO_3$ solution infiltration until the targeted amount of silver was obtained. Then the cell was calcined at 500 °C for 5 h to decompose the $AgNO_3$ into metallic silver. The amount of infiltrated silver was determined based on the weight difference between the cell before the infiltration process and that of the cell after infiltration and calcination. In this study, the silver content in the cathode was controlled at approximately 45 wt.%.

A three-electrode cell with the configuration shown in Fig. 2 was used for the electrode polarization test. To create the cell, a Pt electrode with the same shape as the WE was painted symmetrically on the other side of the SDC electrolyte pellet and fired at 900 °C in air for 30 min to act as a counter electrode (CE). A silver (DAD-87, Shanghai Research Institute of Synthetic Resins, Shanghai, China) electrode encircled the counter electrode to act as a reference electrode (RE). The gap between the counter and reference electrodes was approximately 3.95 mm to prevent systematic errors in the electrochemical measurements.

2.2. Characterization

The phase structure of the samples was analyzed via powder X-ray diffraction using a diffractometer (Bruker D8 Advance) that operates using Cu Kα radiation (λ = 1.5418 Å). Diffraction patterns were determined at room temperature by step scanning angles (2θ) between 20° and 80°. The microscopic features of the sintered electrodes were determined using an Environmental Scanning Electron Microscope (ESEM, QUANTA-2000) equipped with an EDX detector. Thermal expansion properties were measured from room temperature to 800 °C in air at a heating rate of 5 °C min^{-1} using a Netsch DIL 402C/S/G dilatometer.

The coking resistance of Ni + SDC, SDC and Ag–SDC was analyzed as follows. The materials in powder form were first treated in a pure CO atmosphere at 800 °C for 5 h. Then a temperature-programmed oxidation (O_2-TPO) analysis was conducted. Any carbon formed on the surface of the materials would be oxidized into CO_2 by the oxygen in the atmosphere during the heating process. We put the effluent gas into an on-line Hiden QIC-20 mass spectrometer to monitor its CO_2 concentration.

2.3. Electrochemical test

Electrochemical impedance spectroscopy (EIS) was measured using a Solartron 1260 frequency response analyzer in combination with a Solartron 1287 potentiostat. The measurements were conducted for a frequency range of 10^{-1} to 10^5 Hz and signal amplitude of 10 mV. Area specific resistance (ASR) of the electrode was calculated from the EIS. The oxygen partial pressure of the surrounding atmosphere during the EIS measurement process was controlled at 0.04–1 atm by mixing O_2 and N_2 with the help of mass flow controllers. The impedance data were collected using a ZView 2.9 software interfaced with a computer data acquisition system and were fitted using a complex non-linear least squares (CNLS) fitting program. The cathodic overpotential was measured using a Solartron 1287 potentiostat/galvanostat and Corrware 2.9 c software. The *IR* drop values originating from the electrolyte and lead/contact resistance levels were combined with the EIS data to establish the *IR*-free I/E data. The exchange current density, i_0, is a direct reflection of the amount of intrinsic electrocatalytic activity and was calculated using the Bulter–Volmer equation:

$$i = i_0 \left[\exp\left(\frac{\alpha_a F\eta}{RT}\right) - \exp\left(\frac{-\alpha_c F\eta}{RT}\right) \right] \quad (1)$$

In high field overpotential, anodic reactions can be ignored, and i_0 can be obtained from the y-intercept of a plot of $\log i$ vs. η. Thus, i_0 was calculated using the following equation:

$$\log i = \log i_0 - \frac{\alpha_c nF}{2.303RT}\eta \quad (2)$$

where η (V) is the cathodic overpotential, α_c is the cathodic coefficient, n is the total number of electrons transferred, F (C mol^{-1}) is the Faraday constant, R (J K^{-1} mol^{-1}) is the gas constant and T (K) is the absolute temperature.

The cathodic coefficient can be calculated using the equation:

$$\alpha_c = \frac{\gamma}{\nu + \gamma\beta} \quad (3)$$

where γ, r and β are the number of electrons transferred before the rate limiting step, the number of electrons transferred during the rate-limiting step, and the symmetry coefficient (typically assumed to be 0.5), respectively.

The performance of the symmetric fuel cells was tested at an in-lab SOFC test station. To create the fuel cell reactor, the cell was affixed to the top of a quartz tube using silver paste. Three percent water humidified (3% H_2O) hydrogen or methane was fed into the anode at a flow rate of 60 ml min^{-1} [STP], with ambient air used as the cathode atmosphere. A thermocouple was positioned near the cathode surface to control and monitor temperature. *I–V* polarization tests were based on a four-probe configuration and were measured using a digital source meter (Keithley 2420).

3. Results and discussion

3.1. Cell morphology

A representative SEM image of the constructed single cell with symmetric Ag–SDC electrodes is shown in Fig. 3a, with photos of the electrodes at a higher magnification level provided in Fig. 3b–d. The SDC electrolyte was dense, with a thickness of approximately 400 μm, and both electrodes had a thickness of approximately 20 μm. We could find no Ni residues throughout both of the electrodes by using EDX which suggested Ni could be perfectly removed from the electrode by dipping it in the HNO_3 solution. The electrodes were still in a highly porous structure after the silver phase

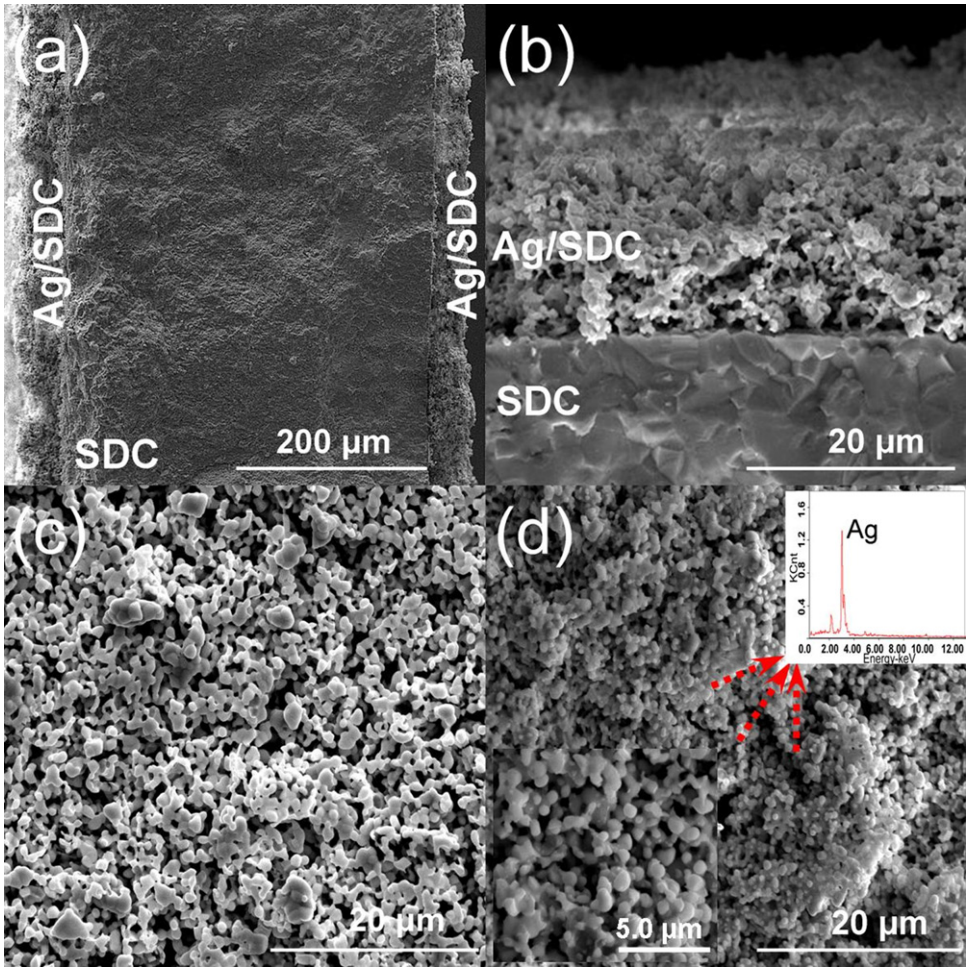

Fig. 3. (a) SEM images of a symmetric cell, (b) the interface between the Ag/SDC electrode and the SDC electrolyte, (c) the SDC scaffold surface before the Ag infiltration process, and (d) the SDC scaffold surface after the Ag infiltration process and heat treatment.

is introduced by infiltration. The silver particles are spherical and have a size of 0.6 μm. They adhered firmly to the SDC electrolyte surface and formed a percolation phase.

As previously mentioned, ideal electrodes for fuel cells should exhibit high electrical conductivity levels to ensure efficient current collection. Otherwise, there may be a large volume of contact resistance. The surface conductivity of the silver-infiltrated SDC (Ag–SDC) electrodes was measured using a four-probe DC conductivity technique. The conductivity level reached as high as 1.56 S cm^{-1} at room temperature, whereas it was only 2.83×10^{-8} S cm^{-1} for a similar porous SDC scaffold before the silver infiltration process. The effectiveness of the dramatically improved surface conductivity further strongly supports the formation of a percolation phase for the silver added to the porous electrodes.

3.2. Thermal expansion

As previously mentioned, the thermal compatibility of cell components is one of the most important concerns affecting the development of SOFCs. To ensure high levels of operational stability, the TECs of cell components should be made as similar as possible. TEC mismatching may result in slow delimitation of the electrode from the electrolyte surface, causing cell performance to worsen. The TECs for conventional composite electrodes typically vary with the weighted average TEC of the individual components. For example, when Datta et al. synthesized and characterized gadolinia-doped ceria-silver cermet cathode material for SOFCs, they observed that the TECs of the cermets increased with the silver content [6]. However, for composites formed by infiltration, it was demonstrated that the TECs were more similar to that of the scaffold than to the weighted average TEC because the scaffold provided the mechanical support for the composite [35–37]. To obtain information about the thermal expansion behavior of the silver-infiltrated SDC porous electrode, a similar 45 wt.% Ag-impregnated porous SDC bar was prepared, and its thermal expansion behavior was measured. The results are shown in Fig. 4; for comparison, the TEC curves of dense SDC are also presented. The calculated TECs at temperatures between 30 and 800 °C from thermal expansion curves are 12.0×10^{-6} and 11.9×10^{-6} K^{-1} for the Ag–SDC and SDC, respectively. As expected, the almost identical TEC values for impregnated Ag–SDC and SDC strongly indicate that the thermal expansion behavior of silver-infiltrated SDC is determined mainly by the porous SDC scaffold.

3.3. Electrode performance

To evaluate the performance of the Ag–SDC composite as a SOFC cathode, the EIS values of the three-electrode cells with the configuration shown in Fig. 2 were first measured in air under open circuit conditions at various temperatures. Before the measurements were conducted, the cells were polarized at −0.4 V in air at 750 °C for 2 h to stabilize the performance of the electrodes. Gold paste was used as the current collector to minimize its

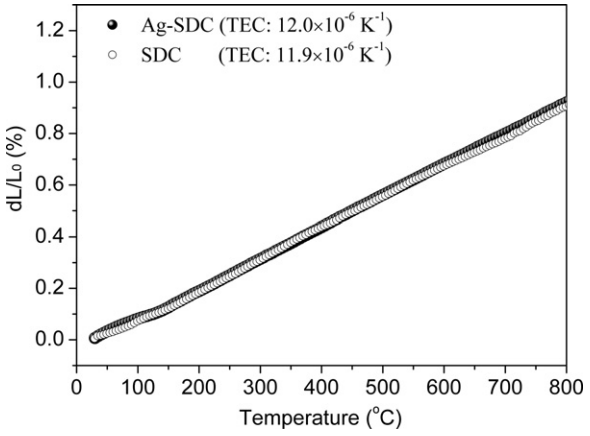

Fig. 4. Thermal expansion curves for the SDC and Ag/SDC bars.

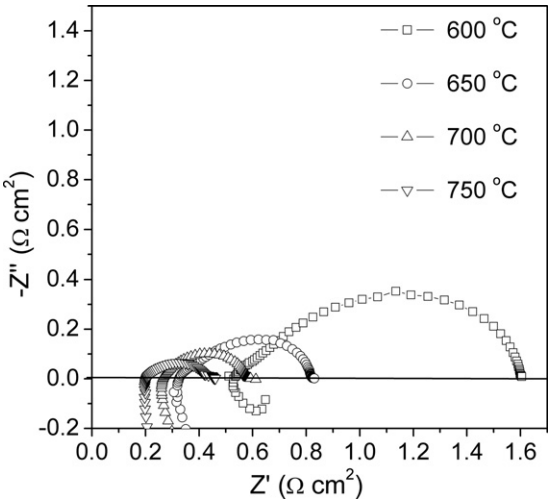

Fig. 5. EIS plots of the cell at various temperatures in air after polarization at 200 mA cm^{-2} at 750 °C for 1 h.

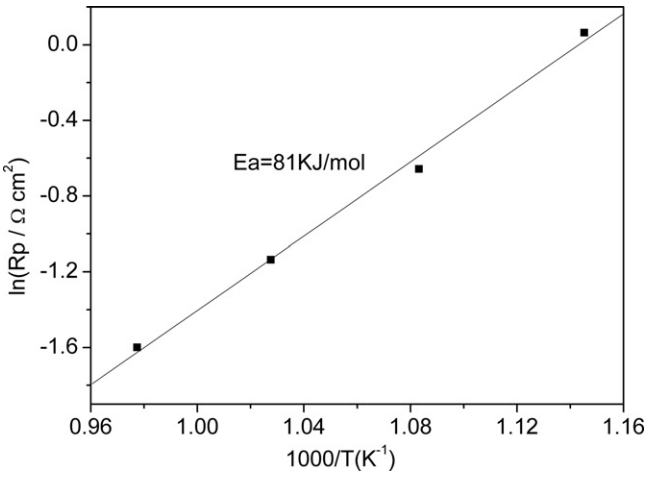

Fig. 6. Temperature dependence of R_p of Ag/SDC in air between 600 and 750 °C.

electrocatalytic contribution of the current collector to the performance of the electrodes. As shown in Fig. 5, ASRs of 0.25, 0.33, 0.51 and 1.07 Ω cm^2 were obtained at 750, 700, 650 and 600 °C, respectively. This shows that the Ag–SDC electrode is highly active for oxygen reduction at intermediate temperatures. In addition, based on the temperature dependence of the ASRs as shown in Fig. 6,

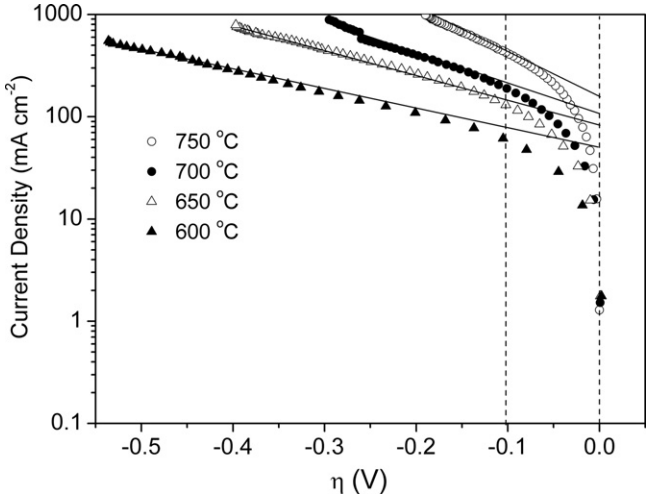

Fig. 7. IR-corrected Tafel plot for the symmetric cell tested in air atmosphere.

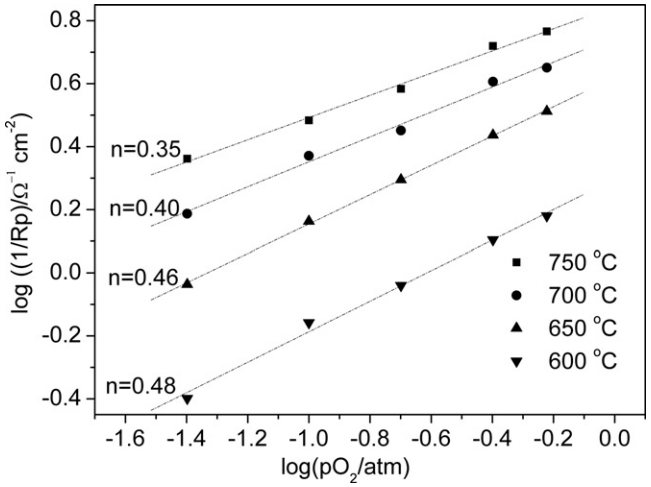

Fig. 8. Representative profiles for the pO_2 dependence of the Ag/SDC electrode at various temperatures.

activation energy (E_a) level of only 81 kJ mol^{-1} was calculated for oxygen reduction over the Ag–SDC electrode. This figure is much lower than the values of 110–130 kJ mol^{-1} reported for many electrodes based on mixed conductors or composite electrodes [8,9]. Several other researchers have also demonstrated the high activity levels of silver cermet cathodes for oxygen reduction [17–19].

Fig. 7 shows the cathodic overpotential curves in *IR*-corrected Tafel plots for the infiltrated Ag–SDC electrode at various temperatures. The overpotential is −100 mV for the Ag–SDC electrode at current density levels of 428.2, 196.1, 129.0 and 59.1 mA cm^{-2} at 750, 700, 650 and 600 °C in air, respectively. The exchange current density (I_o), which is a direct reflection of intrinsic electro-catalytic activity, was calculated using the Bulter–Volmer equation using the high field overpotential. The values obtained were 161.1, 115.1, 90.3 and 38.7 mA cm^{-2} at 750, 700, 650 and 600 °C, respectively. By comparison, the reported exchange current density of conventional LSM electrodes is only ~9 mA cm^{-2} at 700 °C [38,39]. Thus, silver-impregnated porous SDC is shown to be an appropriate oxygen reduction electrode for use at intermediate temperatures.

To obtain more information about oxygen reduction over the infiltrated Ag–SDC electrode, we also measured the EIS values of the electrode under different oxygen partial pressure levels at various temperatures. It emerged that $\log(1/R_p)$ can be fitted linearly to $\log P_{O_2}$; the results are shown in Fig. 8. The value of slope (n) is

closely related to the processes that occurred over the electrode. A slope of 1 should be expected if the rate-limiting step in the oxygen reduction process is gas-phase diffusion within the pores of the Ag–SDC electrodes at a ratio of 1/2 for the dissociation adsorption of O_2 over the electrode surface ($O_2 \rightarrow 2O_{ad}$), 3/8 for the reduction of surface-adsorbed O_{ad} species to O_{ad}^- ($O_{ad} + e^- \rightarrow O_{ad}^-$), and 1/4 for the charge transfer process ($O_{ad}^- \rightarrow O_{TPB}^-$) [40]. An increase in the value of the slope from ~3/8 (0.35) at 750 °C to ~1/2 (0.48) at 600 °C was observed in this study. These results indicate that with a decrease in operating temperatures from 750 to 600 °C, a transition occurs in the rate determination step for oxygen reduction from the reduction of surface-adsorbed O_{ad} species to O_{ad}^- to oxygen dissociative adsorption.

To test the performance of the infiltrated Ag–SDC composite as an anode of SOFCs, we also measured the EIS of a three-electrode cell under different anodic polarization current densities at various temperatures in a 3% water humidified hydrogen atmosphere. Selected results are shown in Fig. 9. A decrease in ASR was observed at all investigated temperatures in tandem with an increase in the polarization current, suggesting that anodic performance improved under anodic polarization. The ASRs under zero anodic polarization current density are 0.35, 0.63, 1.33 and 3.15 Ω cm^2 at 750, 700, 650 and 600 °C, respectively, whereas the ASRs decreased to 0.33, 0.43, 0.61, and 1.12 Ω cm^2 at corresponding temperatures under an anodic polarization current density of 0.03 A cm^{-2}. The above results indicate that the silver-infiltrated porous SDC electrode also performs well as an anode of SOFC operating between 750 and 600 °C.

Table 1
Resistances of the cell at various temperatures with H_2 as fuel.

T (°C)	R_Ω (Ω cm^2)	R_E (Ω cm^2)	R_C (Ω cm^2)	R_A (Ω cm^2)
600	1.585	3.126	1.070	2.056
650	0.980	1.359	0.505	0.854
700	0.649	0.591	0.328	0.263
750	0.422	0.288	0.257	0.031

3.4. Single cell performance

A complete symmetric cell with a 400 μm thick SDC electrolyte and 45 wt.% silver-impregnated porous SDC electrodes (20 μm) was then subjected to a power generation test. During the test, one Ag–SDC electrode was exposed to ambient air while the other Ag–SDC electrode was used with 3% water humidified hydrogen Fig. 10 shows the *I–V* and *I–P* curves at various temperatures. A peak power density (PPD) of 200 mW cm^{-2} was achieved at 750 °C, and the power density was 35 mW cm^{-2} at 600 °C. These results are highly encouraging given the thick electrolyte (0.4 mm) used in this study. Table 1 lists the ohmic resistance (R_Ω) of the cell and

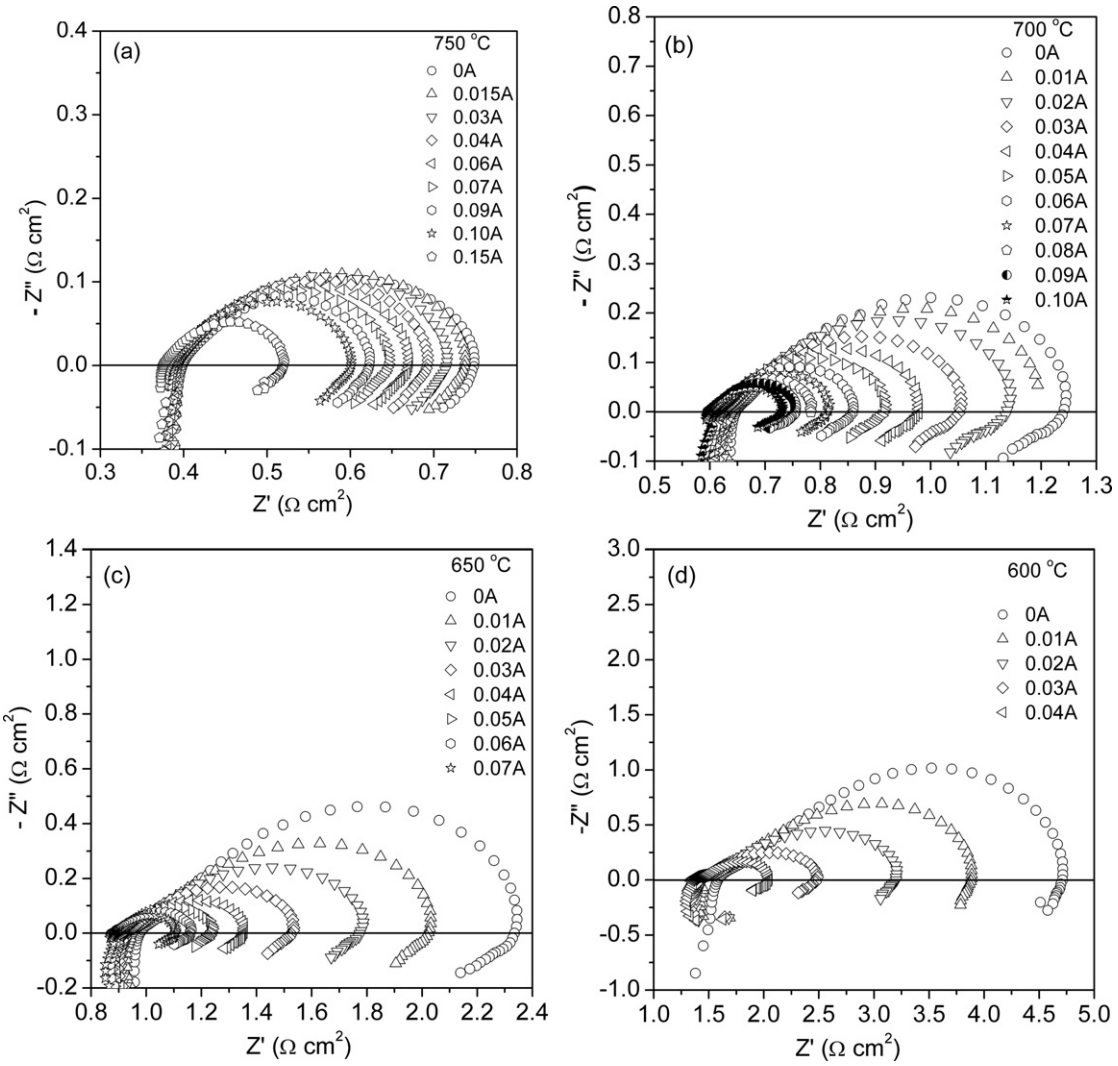

Fig. 9. EIS plots for the three-electrode cell under different anodic polarization current densities at various temperatures in a 3% water humidified hydrogen atmosphere.

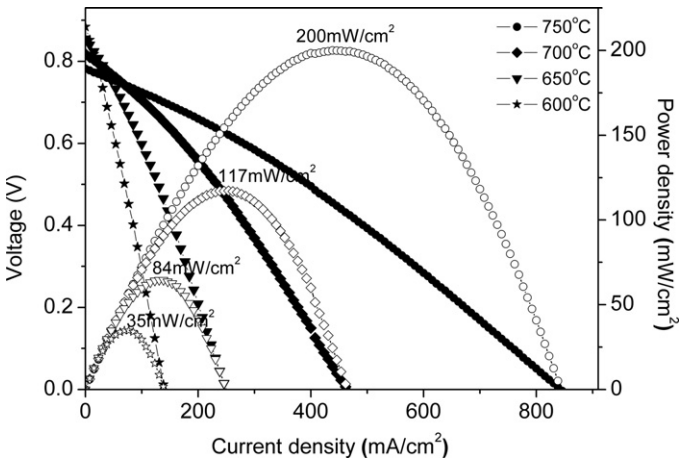

Fig. 10. *I–V* and *I–P* curves of the cells operating on hydrogen fuel.

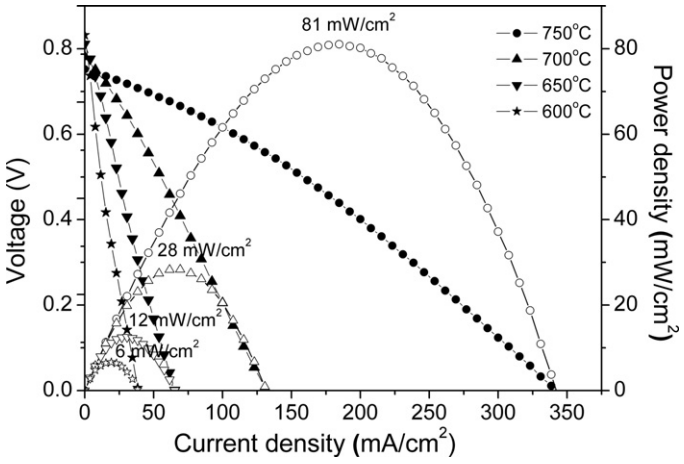

Fig. 11. *I–V* and *I–P* curves of the cells operating on CO fuel.

the overall electrode polarization resistance (R_E) at various operating temperatures measured using the EIS values under open-circuit conditions. For comparison purposes, the cathodic polarization resistance (R_C) levels, measured based on the symmetric cell configuration, are also presented. The anodic polarization resistance (R_A) levels were roughly calculated by subtracting the cathodic polarization resistance from the total electrode polarization resistance; these results are also listed in Table 1. The anodic polarization resistance levels exhibited greater temperature dependence than the cathodic polarization resistance levels.

Recently, it was demonstrated that physically mixed Ag and GDC composites also perform well as a SOFC anode when CO fuel is used [19]. This may mean that a symmetric cell with infiltrated Ag–SDC electrodes could also operate on reforming hydrocarbon gases. Fig. 11 shows the *I–V* and *I–P* curves of the same cell operating on CO fuel at various temperatures. We observed lower cell power outputs than those obtained when hydrogen was used. This finding suggests that CO is associated with a slower electrochemical oxidation rate for the Ag–SDC electrode. In any event, the cell still performed acceptably well, and a PPD of 81 mW cm^{-2} was obtained at 750 °C.

3.5. Coke resistance

One of the most serious problems with conventional SOFCs with nickel cermet anodes operating on carbon-containing fuels is coke formation, which may lead to the rapid deterioration of cell performance over time. The coking resistance of the infiltrated Ag–SDC electrode was investigated by first treating an Ag–SDC powder crashed from an infiltrated Ag–SDC electrode in a pure CO atmosphere at 800 °C for 5 h and then conducting an O_2-TPO analysis. Fig. 12 provides the O_2-TPO profile with the CO_2 signal of the Ag–SDC composite after CO exposure. For comparison purposes, the same investigation was also conducted for the Ni + SDC anode and pure SDC. For all tests, the sample weight was 0.01 g. The ratio of the CO_2 peak areas for Ag–SDC:SDC:Ni–SDC was found to be 1.0:1.85:30.9. This clearly shows that the infiltrated Ag–SDC composite has much better coke resistivity than the Ni + SDC cermet. Furthermore, any carbon formed over the anode can be easily eliminated by changing the gas flows because bulk silver will not oxidize very much at elevated temperatures.

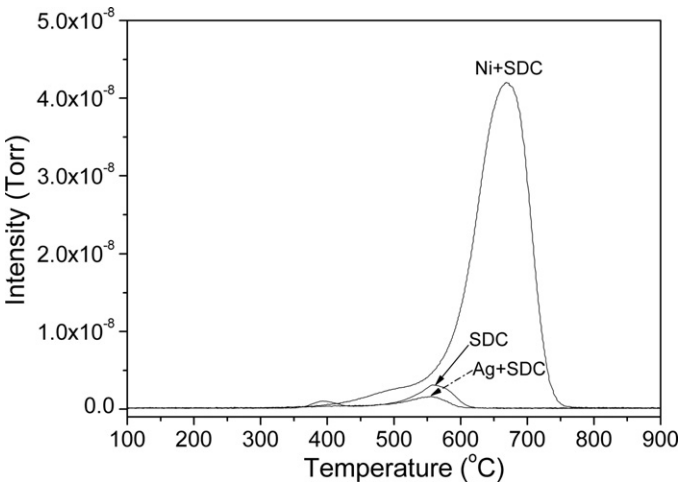

Fig. 12. O_2-TPO profiles with CO_2 signal for Ni + SDC, SDC, and Ag/SDC.

4. Conclusions

In this paper, symmetric SOFC with a whole cell constructed using a samaria-doped ceria framework has been successfully presented. All key components of this technology exhibit similar thermal expansion behavior, and the cell fabrication and maintenance processes are simple. In addition, the technology performs well at intermediate temperatures. The use of silver as the electrocatalyst effectively prevented coke formation over the anode when CO fuel was used. In addition, any deposited carbon can easily be eliminated by simply changing the gas flow. The consistent thermal expansion of the cell components, the excellent coke resistance of the technology, the simple cell configuration, and the attractive cell power output suggest that this technology may be useful in many fields.

Acknowledgements

This work was supported by the “National Science Foundation for Distinguished Young Scholars of China” under contract No. 51025209, the New Century Excellence Program of Chinese Ministry of Education, and SAIT, Samsung Electronics Co., Ltd, Korea.

References

[1] N.Q. Minh, T. Takahashi, Science and Technology of Ceramic Fuel Cells, Elsevier, Amsterdam, The Netherlands, 1995.
[2] C. Su, Y.Z. Wu, W. Wang, Y. Zheng, R. Ran, Z.P. Shao, J. Power Sources 195 (2010) 1333–1343.
[3] J.-H. Koh, Y.-S. Yoo, J.-W. Park, H.C. Lim, Solid State Ionics 149 (2002) 157–166.
[4] V. Alzate-Restrepo, J.M. Hill, J. Power Sources 195 (2010) 1344–1351.
[5] D.M. Bastidas, S. Tao, J.T.S. Irvine, J. Mater. Chem. 16 (2006) 1603–1605.

[6] P. Datta, P. Majewski, F. Aldinger, Mater. Chem. Phys. 107 (2008) 370–376.
[7] Y. Huang, K. Ahn, J.M. Vohs, R.J. Gorte, J. Electrochem. Soc. 151 (2004) A1592–A1597.
[8] Z.P. Shao, S.M. Halle, Nature 431 (2004) 170–173.
[9] J.B. Liu, A.C. Co, S. Paulson, V.I. Birss, Solid State Ionics 177 (2006) 377–387.
[10] C.R. Xia, M.L. Liu, Adv. Mater. 14 (2002) 521–523.
[11] E.P. Murray, T. Tsai, S.A. Barnett, Nature 400 (1999) 649–651.
[12] S. Park, J.M. Vohs, R.J. Gorte, Nature 404 (2000) 265–267.
[13] T. Hibino, A. Hashimoto, T. Inoue, J.-I. Tokuno, S.-I. Yoshida, M. Sano, Science 288 (2000) 2031–2033.
[14] T. Hibino, A. Hashimoto, M. Yano, M. Suzuki, M. Sano, Electrochim. Acta 48 (2003) 2531–2537.
[15] N.Q. Minh, J. Am. Ceram. Soc. 76 (1993) 563–588.
[16] B.C.H. Steele, A. Heinzel, Nature 414 (2001) 345–352.
[17] Y. Lin, R. Ran, Z.P. Shao, Int. J. Hydrogen Energy 35 (2010) 8281–8288.
[18] S.P. Simner, M.D. Anderson, J.E. Coleman, J.W. Stevenson, J. Power Sources 161 (2006) 115–122.
[19] F.-Y. Wang, S. Cheng, B.-Z. Wan, Catal. Commun. 9 (2008) 1595–1599.
[20] H. Nakano, S. Kawakami, T. Fujitani, J. Nakamura, Surf. Sci. 454–456 (2000) 295–299.
[21] H. Kim, S. Park, J.M. Vohs, R.J. Gorte, J. Electrochem. Soc. 148 (2001) A693–A695.
[22] S.W. Tao, J.T.S. Irvine, Nat. Mater. 2 (2003) 320–323.
[23] J.C. Ruiz-Morales, J. Canales-Vázquez, J. Peña-Martínez, D.M. López, P. Núñez, Electrochim. Acta 52 (2006) 278–284.
[24] J. Canales-Vázquez, J.C. Ruiz-Morales, D. Marrero-López, J. Peña-Martínez, P. Núñez, P. Gómez-Romero, J. Power Sources 171 (2007) 552–557.
[25] J.C. Ruiz-Morales, J. Canales-Vázquez, B. Ballesteros-Pérez, J. Peña-Martínez, D. Marrero-López, J.T.S. Irvine, P. Núñez, J. Eur. Ceram. Soc. 27 (2007) 4223–4227.
[26] J.C. Ruiz-Morales, H. Lincke, D. Marrero-López, J. Canales-Vázquez, P. Núñez, Bol. Soc. Esp. Ceram. Vidrio 46 (2007) 218–223.
[27] A. El-Himri, D. Marrero-López, J.C. Ruiz-Morales, J. Peña-Martínez, P. Núñez, J. Power Sources 188 (2009) 230–237.
[28] Y. Zheng, C.M. Zhang, R. Ran, R. Cai, Z.P. Shao, D. Farrusseng, Acta Mater. 57 (2009) 1165–1175.
[29] Q. Liu, X. Dong, G. Xiao, F. Zhao, F. Chen, Adv. Mater. 22 (2010) 5478–5482.
[30] K. Kerman, B.K. Lai, S. Ramanathan, J. Power Sources 196 (2011) 2608–2614.
[31] S.W. Tao, J.T.S. Irvine, J. Electrochem. Soc. 151 (2004) A252–A259.
[32] J.C. Ruiz-Morales, J. Canales-Vázquez, D. Marrero-López, D. Pérez-Coll, J. Peña-Martínez, P. Núñez, J. Power Sources 177 (2008) 154–160.
[33] S.B. Adler, Chem. Rev. 104 (2004) 4791–4843.
[34] J.R. Wilson, W. Kobsiriphat, R. Mendoza, H.Y. Chen, J.M. Hiller, D.J. Miller, K. Thornton, P.W. Voorhees, S.B. Adler, S.A. Barnett, Nat. Mater. 5 (2006) 541–544.
[35] K. Yamahara, C.P. Jacobson, S.J. Visco, L.C. De Jonghe, Solid State Ionics 176 (2005) 451–456.
[36] S.P. Jiang, Mater. Sci. Eng. A 418 (2006) 199–210.
[37] J.M. Vohs, R.J. Gorte, Adv. Mater. 21 (2009) 943–956.
[38] S.P. Jiang, Solid State Ionics 146 (2002) 1–22.
[39] Z.Y. Jiang, L. Zhang, L. Cai, C. Xia, Electrochim. Acta 54 (2009) 3059–3065.
[40] S.-W. Baek, J. Bae, Y.-S. Yoo, J. Power Sources 193 (2009) 431–440.